Magnetic Dipolar Ordering and Quantum Phase Transition in an Fe_8 Molecular Magnet

E. Burzurí,[1] F. Luis,[1,*] B. Barbara,[2] R. Ballou,[2] E. Ressouche,[3] O. Montero,[1] J. Campo,[1] and S. Maegawa[4]

[1]*Instituto de Ciencia de Materiales de Aragón, C.S.I.C.-Universidad de Zaragoza, and Departamento de Física de la Materia Condensada, Universidad de Zaragoza, E-50009 Zaragoza, Spain*
[2]*Institut Néel, CNRS & Université Joseph Fourier, BP 166, 38042 Grenoble Cedex 9, France*
[3]*CEA/Grenoble, INAC/SPSMS-MDN, 17 rue des Martyrs, 38054 Grenoble Cedex 9, France*
[4]*Graduate School of Human and Environmental Studies, Kyoto University, Kyoto 606-8501, Japan*

(Received 27 December 2010; published 23 August 2011)

We show that a crystal of mesoscopic Fe_8 single-molecule magnets is an experimental realization of the quantum Ising model in a transverse field, with dipolar interactions. Quantum annealing has enabled us to explore the quantum and classical phase transitions between the paramagnetic and ferromagnetic phases, at thermodynamical equilibrium. The phase diagram and critical exponents that we obtain agree with expectations for the mean-field universality class.

DOI: 10.1103/PhysRevLett.107.097203 PACS numbers: 75.50.Xx, 73.43.Nq, 75.40.Gb, 75.45.+j

Quantum phase transitions (QPTs) [1,2] have been extensively studied in recent years. Physical realizations include the superconductor insulator transition in cuprates [3–5], the onset of antiferromagnetism in heavy fermions [6], the pressure-driven insulator-metal transition in V_2O_3 [7], and the magnetic transitions driven by field ($LiHoYF_4$ [8]) or concentration (Cr_xV_{1-x} alloys [9]). In addition to their intrinsic interest, a plethora of new properties arise at nonzero temperature.

In magnetism, the archetypal QPT is realized by a lattice of N coupled Ising spins in a transverse magnetic field $H_\perp$ [10], the Hamiltonian of which reads as follows:

$$\mathcal{H} = -2S^2 \sum_{i<j}^{N} J_{ij}\sigma_i^z\sigma_j^z - \Delta_S \sum_{i}^{N} \sigma_i^x. \qquad (1)$$

Here, σ's are the Pauli spin operators, J_{ij} the longitudinal couplings (here of dipolar origin), and Δ_S the ground-state tunnel splitting which depends on and vanishes with $H_\perp$. The classical long-range order that exists for $H_\perp = \Delta_S = 0$ (ferromagnetic or antiferromagnetic) competes with the field-induced quantum fluctuations ($[\mathcal{H}, \sigma] \neq 0$). It is completely destroyed at the critical point when $\Delta_S(H_\perp) \gtrsim \Delta_{Sc}$, where $\Delta_{Sc} = 2JS^2 \sim k_B T_c$, $J = (1/N)\sum_{i<j} J_{ij}$, and T_c is the Curie temperature. The ground state becomes then a superposition of "up" and "down" spin states.

Crystals of lanthanide-based insulators seem to be natural candidates to observe a QPT [8,11]. Because of the weak interactions, quantum fluctuations can become noticeable at moderate transverse fields. However, the strong hyperfine interactions seriously limit the observation of the intrinsic quantum criticality in these materials [12,13]. Single-molecule magnets (SMMs) based on $3d$ transition metals show some properties that make them better suited for such QPT studies: Dipolar interactions are weak because of the very large intermolecular distances [14], and hyperfine interactions are also generally weak enough not to block the QPT. Finally, SMMs show phenomena, like tunneling [15], interference [16], and superpositions of spin states [17], which reveal the existence of important quantum spin fluctuations. Yet, the search for a QPT faces some experimental challenges, mainly associated with structural disorder. In Mn_{12} acetate, where indications of a possible QPT were inferred from magnetic neutron diffraction experiments [18], the local anisotropy axes are slightly tilted due to the presence of several isomers giving rise, in the presence of a perpendicular field, to random fields [19]. It has been argued [20] that such fields turn Mn_{12} acetate into a realization of the classical random-field Ising model. The existence of a pure QPT in a crystal of molecular nanomagnets is, therefore, not yet established. Our aim here is to explore the experimental realization of the Ising QPT model in a crystal of Fe_8 SMMs [21] where (i) classical Monte Carlo (MC) simulations suggest a ferromagnetic ground state with $T_c = 0.54$ K [22,23], (ii) hyperfine frequencies, much smaller than Larmor frequencies, cannot perturb quantum dynamics of SMMs, and (iii) disorder is weak enough to avoid sizable random fields.

Each Fe_8 molecule (brief for $[(C_6H_{15}N_3)_6Fe_8O_2(OH)_{12}]$) has a spin $S = 10$ and a strong uniaxial magnetic anisotropy. In the presence of a magnetic field $\vec{H}$, the magnetism of Fe_8 can be described by the following spin Hamiltonian:

$$\mathcal{H}_0 = -DS_z^2 + E(S_x^2 - S_y^2) - g\mu_B \vec{H}\,\vec{S}, \qquad (2)$$

where $D/k_B = 0.294$ K, $E/k_B = 0.046$ K, and $g = 2$ [21]. Equation (2) defines x, y, and z as the hard, medium, and easy magnetization axes, respectively. In the triclinic structure of Fe_8, these axes are common to all molecules [24].

Susceptibility experiments were performed on a 1.6 mg single crystal [24] of approximate dimensions $1 \times 2 \times 1\ \mathrm{mm}^3$. The complex magnetic susceptibility $\chi = \chi'(T,\omega) - i\chi''(T,\omega)$ was measured down to 90 mK and in the frequency range 3 Hz $\leq \omega/2\pi \leq$ 20 kHz by using a homemade ac susceptometer thermally anchored to the mixing chamber of a ^{3}He-^{4}He dilution refrigerator. The

magnetic field $\vec{H}$ was applied with a 9 T × 1 T × 1 T superconducting vector magnet.

The magnetic anisotropy axes were first approximately located by x-ray diffraction, by using the information reported in Ref. [24]. The magnetic easy axis z was oriented parallel to the ac excitation magnetic field of amplitude $h_{ac} = 0.01$ Oe. The precise alignment of $\vec{H}$ perpendicular ($\pm 0.05°$) to z and close ($\pm 20°$) to the medium y axis was done at low temperatures ($T = 2.6$ K), by using the strong dependence of $\chi'(T, \omega)$ on the magnetic field orientation [25]. The sample was completely covered by a nonmagnetic epoxy to prevent it from moving under the action of $\vec{H}$.

Neutron diffraction experiments were performed on the thermal neutron two-axis diffractometer D23 at the Institute Laue Langevin. A single crystal, thermally anchored to the mixing chamber of a ^{3}He-^{4}He dilution refrigerator ($T \geq 50$ mK), was mounted so as to have z orthogonal to $\vec{H}$. In this experiment, $\vec{H}$ was close to the hard axis x. Longitudinal field components arising from the nonperfect orientation of the crystal were compensated by means of a superconducting minicoil inserted in the space between the dilution refrigerator and the superconducting magnet. The intensities of different Bragg peaks, in particular, (010), (−100), and (−212), were measured as a function of T (under a constant $H_\perp$) and $H_\perp$ (for a constant T). The nonmagnetic contributions were measured at high T (5 K) and $H_\perp = 0$. The fit of the magnetic intensities enabled us to estimate the magnetization components along the external magnetic field $M_\perp$ and along the anisotropy axis M_z.

The ac susceptibility (Fig. 1) deviates from equilibrium for low $H_\perp$ and low T, as shown by the vanishing of χ' and by the relatively large values of χ''. The superparamagnetic blocking temperature T_b (associated with the χ'' maximum) strongly depends on frequency (not shown). In these dipolar Ising-like systems, out-of-equilibrium conditions arise from the presence of energy barriers larger than the typical interaction energies (i.e., $T_b > T_c$), a situation which can be inverted by quantum annealing via the application of $H_\perp$ [26,27]. When $H_\perp$ increases, the height of the energy barrier decreases and spins are able to tunnel via lower energy states, which leads to enhanced spin-lattice relaxation rates. This explains the decrease of T_b, as shown in the inset in Fig. 1(a). Besides enhancing the spin dynamics, the magnetic field also lowers the paramagnetic susceptibility. This decrease can be associated with the reduction of the effective S_z by quantum fluctuations as well as with the decrease in the paramagnetic Weiss temperature (see below and Ref. [25]). Both effects become more noticeable for $H_\perp \gtrsim 1$ T, as seen in Fig. 1(a).

At moderate $H_\perp$, e.g., at $\mu_0 H_\perp = 1.7$ T, χ' is not fully out of equilibrium. The relaxation time $\tau = \chi''/\chi'\omega$ at the same field is already very short, and, more importantly, it remains constant below approximately 0.25 K [inset in Fig. 1(b)]. χ' becomes independent of frequency, and thus

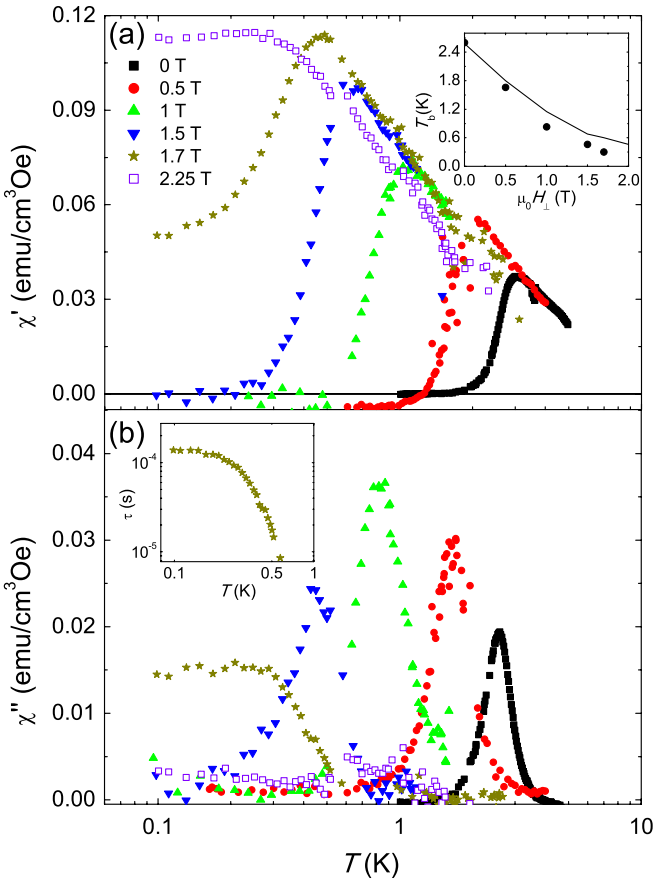

FIG. 1 (color online). χ' (a) and χ'' (b) measured at $\omega/2\pi = 333$ Hz and different $H_\perp$. The inset in (a) shows the shift of χ'' maxima with increasing $H_\perp$. The solid line shows theoretical predictions for quantum spin-phonon relaxation that follow from Pauli's master equation as described in Ref. [31]. The inset in (b) shows the magnetic relaxation time at $\mu_0 H_\perp = 1.7$ T.

it reaches full equilibrium, for $\mu_0 H_\perp \gtrsim 2$ T as seen in Fig. 2(a).

We next show the existence of a magnetic phase transition and discuss its critical behavior. As shown in Fig. 2(a), $1/\chi'$ follows the Curie-Weiss law at sufficiently high T, becoming independent of T below 0.34 K (which we take as the critical temperature T_c at this field $\mu_0 H_\perp = 2.25$ T). The saturation value $1/\chi_{max} = 9.5(5)$ cm^3 Oe/emu agrees well with the demagnetizing factor of our sample $N = 10(1)$ cm^3 Oe/emu, as expected for an equilibrium ferromagnetic phase transition. A very similar behavior is observed as $H_\perp$ is varied at constant T [Fig. 2(b)]. Again, $1/\chi'$ depends linearly on $H_\perp$ until it saturates (to the same value $\simeq N$) below $\mu_0 H_c = 2.65(5)$ T, which we take as the critical magnetic field. The intrinsic susceptibility χ_i', corrected from demagnetizing effects, is plotted vs the reduced temperature (at 2.33 T) and field (at 0.11 K) in Fig. 2(c). Under these conditions, χ_i' should follow, as it approximately does, the power laws

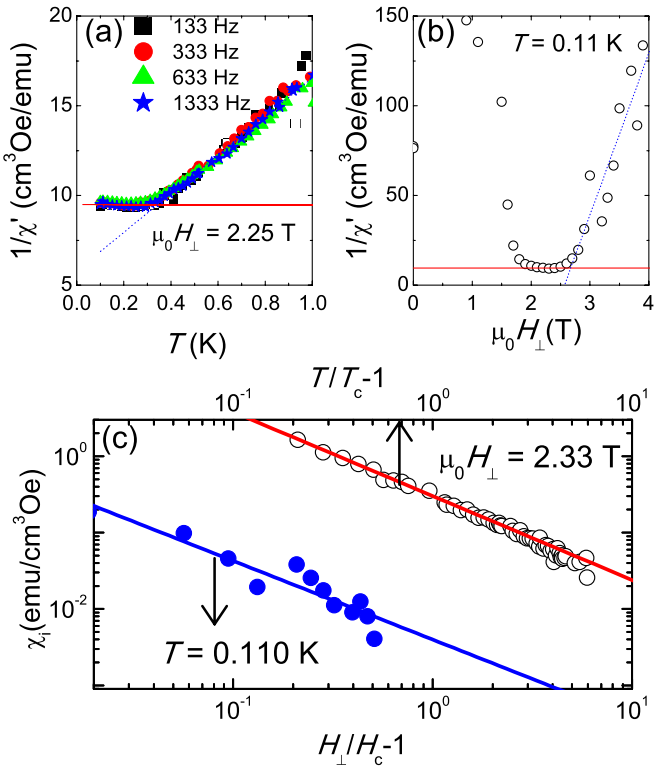

FIG. 2 (color online). (a),(b) $1/\chi'$ measured at $\mu_0 H_\perp = 2.25$ T as a function of T and at $T = 0.110$ K as a function of $H_\perp$, respectively. The crossovers between the "Curie-Weiss" law, observed at either high T or high $H_\perp$ (dotted blue lines), and the ferromagnetic limit $1/\chi' = N$ (solid red lines) give T_c [$= 0.34(1)$ K] and $\mu_0 H_c$ [$= 2.65(5)$ T], respectively. (c) Log-log plot of demagnetization-corrected χ_i' vs the reduced temperature (for $\mu_0 H_\perp = 2.33$ T with $T_c = 0.31$ K, ○) and field (at $T = 0.110$ K with $\mu_0 H_c = 2.65$ T, ●). The linear fits give critical exponents $\gamma_{cl} \simeq 1.1(1)$ and $\gamma_{qu} \simeq 1.0(1)$.

$$\chi_i' = \left(\frac{T - T_c}{T_c}\right)^{-\gamma_{cl}}, \qquad \chi_i' = \left(\frac{H_\perp - H_c}{H_c}\right)^{-\gamma_{qu}}. \tag{3}$$

The slopes give critical exponents $\gamma_{cl} = 1.1(1)$ and $\gamma_{qu} = 1.0(1)$, in good agreement with $\gamma = 1$ of the mean-field universality class. This result agrees with the prediction that the marginal dimensionality for mean-field behavior is $d^* = 3$ in an Ising dipolar ferromagnet [28] and with the fact that the critical exponents for the field-induced transition at $T \to 0$ become equivalent to those of the classical transition in $(d + 1)$ dimensions [29].

The H_c-T_c phase diagram shown in Fig. 3 was obtained by repeating the different procedures described in Fig. 2. The equilibrium reciprocal susceptibility, measured above T_b, was fitted with a Curie-Weiss law. The extrapolations of these fits to $1/\chi' \to 1/\chi_{max}$ were used to determine either T_c, at fixed $H_\perp$ [Fig. 2(a)], or H_c, at fixed T [Fig. 2(b)]. A third method consisted in using the scaling plots of Fig. 2(c) to determine T_c independently.

The three methods give a very consistent $H_c(T_c)$ curve. As expected, T_c decreases when quantum fluctuations increase (with $H_\perp$). The phase diagram shows a transition induced by thermal fluctuations at $T_c(H_\perp = 0) = 0.60(5)$ K (classical) and a transition induced by quantum fluctuations at $\mu_0 H_c(T = 0) = 2.65(5)$ T (quantum). The ferromagnetic nature of the ordered phase agrees with theoretical predictions [22,23]. The solid line is obtained by solving numerically the mean-field Hamiltonian for the $S = 10$ spin

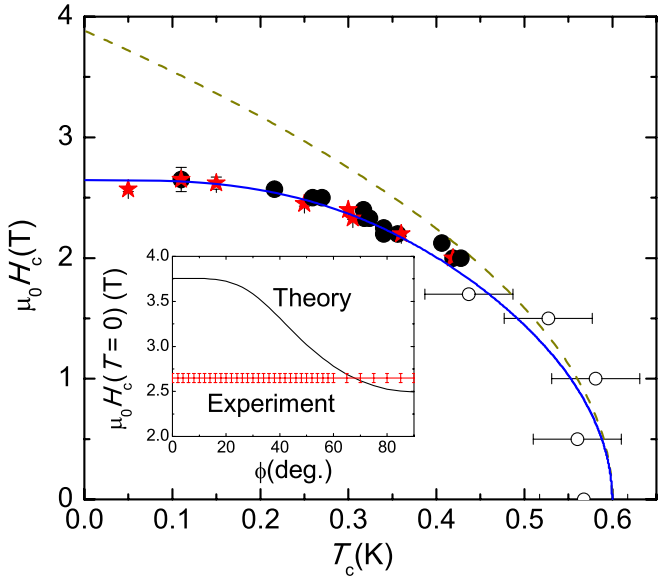

FIG. 3 (color online). H_c-T_c phase diagram determined from the linear extrapolation of $1/\chi'$ to $1/\chi_{max}$, as shown in Figs. 2(a) and 2(b). ● and ○ correspond to $T_c > T_b$ and $T_c < T_b$, respectively; ★, data determined from susceptibility scaling plots, as those shown in Fig. 2(c). Solid line, quantum mean-field calculation of the phase boundary using Eq. (4); dashed line, classical phase diagram, derived from MC simulations. Inset: Zero-temperature critical field vs angle ϕ. The horizontal line represents the experimental $H_c(T_c = 0)$.

$$\mathcal{H} = -DS_z^2 + E(S_x^2 - S_y^2) - g\mu_B H_\perp (S_x \cos\phi + S_y \sin\phi) - 2J\langle S_z\rangle_T S_z, \tag{4}$$

where ϕ is the angle between the magnetic field and the hard axis, $2J$ is the molecular field coefficient, and $\langle S_z\rangle_T$ is the thermal average of S_z. We set $\phi = 68°$ that, as shown by the inset in Fig. 3, accounts for $\mu_0 H_c(T = 0) \simeq 2.65$ T. A very good fit is obtained for $J/k_B = 2.85 \times 10^{-3}$ K, which gives $T_c = 0.6$ K. This value agrees, within 10%, with the Curie temperature $T_c = 0.54$ K determined by classical MC simulations [22]. An extension [30] of these simulations to the case of nonzero $H_\perp$ gives the classical phase boundary (dashed line in Fig. 3), which is well approximated by $H_c(T_c) = H_c(0)[1 - T_c/T_c(H_\perp = 0)]^{1/2}$. In this model $H_c(0)$ equals the anisotropy field $H_K = 2[D - E(\sin^2\phi - \cos^2\phi)]/g\mu_B S \simeq 3.8$ T, which clearly overestimates the experimental critical field due to the absence of quantum fluctuations.

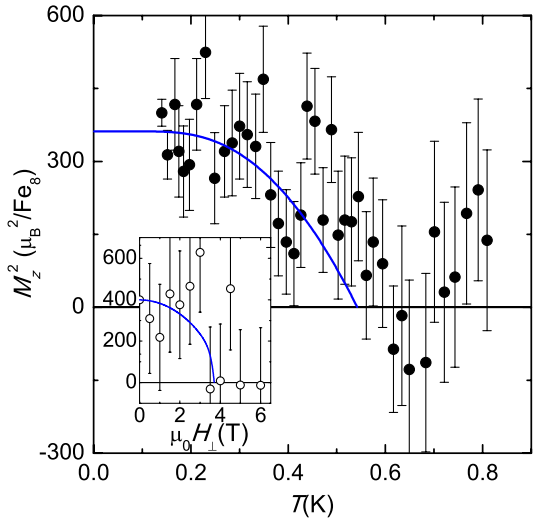

FIG. 4 (color online). Squared longitudinal magnetization of a Fe_8 crystal determined from neutron diffraction intensities measured at $\mu_0 H_\perp = 1.5$ T. The inset shows data measured at $T = 0.14$ K as a function of $H_\perp$. The lines are mean-field calculations using Eq. (4) with $\phi = 0$.

Additional evidence supporting the existence of a transition to a ferromagnetic phase is found in the results of neutron diffraction experiments. Figure 4 shows M_z^2 determined from magnetic diffraction intensities measured at $\mu_0 H_\perp = 1.5$ T. The inset shows field-dependent data measured at $T = 0.14$ K. Despite the high noise level, typical of these experiments, the results show the onset of a net spontaneous M_z in, respectively, the low-T [$\leq 0.6(1)$ K] and low-$H_\perp$ [$\leq 3(1)$ T] regions.

In summary, we have shown that the SMM Fe_8 undergoes a dipolar ferromagnetic to paramagnetic phase transition of (i) classical nature ($\mu_0 H_c = 0$ T and $T_c = 0.6$ K) and (ii) quantum nature ($T_c = 0.11$ K and $\mu_0 H_c = 2.65$ T). Long-range magnetic order was enabled by the use of quantum annealing allowing the spin bath to attain equilibrium despite high energy barriers preventing spin reversal. The H_c-T_c phase diagram and critical exponents are in excellent agreement with results obtained from exact diagonalization of the mean-field Hamiltonian Eq. (4). As expected, the critical behavior belongs to the mean-field universality class of the Ising model in a transverse magnetic field. The classical portion of the phase diagram (near zero field) agrees very well with classical MC calculations, giving, in particular, nearly the same T_c. Deviations of the classical model become important above ~ 2 T, when quantum fluctuations dominate largely over thermal fluctuations.

We are grateful to Julio Fernández for useful suggestions and for sharing with us the results of his classical MC simulations. We acknowledge D10 and the CRG D23 lines of ILL for allocating measuring time for the neutron diffraction experiments. We acknowledge Eric Bourgeat-Lami, Xavier Tonon, Pascal Fouilloux, and Bruno Vettard for their help in designing, fabricating, and installing the superconducting minicoil used in these experiments and Tomoaki Yamasaki and Miki Ueda for the synthesis of the samples. The present work was partly funded by Spanish MICINN Grant No. MAT2009-13977-C03 (MOLCHIP) and Consolider-Ingenio on Molecular Nanoscience.

*fluis@unizar.es

[1] J. A. Hertz, Phys. Rev. B **14**, 1165 (1976).
[2] S. Sachdev, *Quantum Phase Transitions* (Cambridge University Press, Cambridge, England, 1999).
[3] S. Sachdev and J. Ye, Phys. Rev. Lett. **69**, 2411 (1992).
[4] A. V. Chubukov and S. Sachdev, Phys. Rev. Lett. **71**, 169 (1993).
[5] A. Sokol and D. Pines, Phys. Rev. Lett. **71**, 2813 (1993).
[6] Q. Si and F. Steglich, Science **329**, 1161 (2010).
[7] S. A. Carter *et al.*, Phys. Rev. Lett. **67**, 3440 (1991).
[8] D. Bitko, T. F. Rosenbaum and G. Aeppli, Phys. Rev. Lett. **77**, 940 (1996).
[9] A. Yeh *et al.*, Nature (London) **419**, 459 (2002).
[10] R. B. Stinchcombe, J. Phys. C **6**, 2459 (1973).
[11] P. Stasiak and M. J. P. Gingras, Phys. Rev. B **78**, 224412 (2008).
[12] M. Schechter and P. C. E. Stamp, Phys. Rev. B **78**, 054438 (2008).
[13] H. M. Ronnow *et al.*, Science **308**, 389 (2005).
[14] A. Morello *et al.*, Phys. Rev. Lett. **90**, 017206 (2003).
[15] B. Barbara *et al.*, J. Magn. Magn. Mater. **140–144**, 1825 (1995); J. R. Friedman *et al.*, Phys. Rev. Lett. **76**, 3830 (1996); J. M. Hernández *et al.*, Europhys. Lett. **35**, 301 (1996); L. Thomas *et al.*, Nature (London) **383**, 145 (1996); C. Sangregorio *et al.*, Phys. Rev. Lett. **78**, 4645 (1997).
[16] W. Wernsdorfer and R. Sessoli, Science **284**, 133 (1999).
[17] F. Luis *et al.*, Phys. Rev. Lett. **85**, 4377 (2000).
[18] F. Luis *et al.*, Phys. Rev. Lett. **95**, 227202 (2005).
[19] A. Cornia *et al.*, Phys. Rev. Lett. **89**, 257201 (2002).
[20] B. Wen *et al.*, Phys. Rev. B **82**, 014406 (2010).
[21] A. L Barra *et al.*, Europhys. Lett. **35**, 133 (1996).
[22] J. F. Fernández and J. J. Alonso, Phys. Rev. B **62**, 53 (2000); **65**, 189901(E) (2002).
[23] X. Martínez-Hidalgo, E. M. Chudnovsky, and A. Aharony, Europhys. Lett. **55**, 273 (2001).
[24] M. Ueda *et al.*, J. Phys. Soc. Jpn. **70**, 3084 (2001).
[25] See Supplemental Material at http://link.aps.org/supplemental/10.1103/PhysRevLett.107.097203 for further details on the alignment of the magnetic field and the effect of quantum fluctuations on the paramagnetic χ.
[26] T. Kadowaki and H. Nishimori, Phys. Rev. E **58**, 5355 (1998).
[27] J. Brooke *et al.*, Science **284**, 779 (1999).
[28] A. Aharony, Phys. Rev. B **8**, 3363 (1973).
[29] R. J. Elliot, P. Pfeuty, and C. Wood, Phys. Rev. Lett. **25**, 443 (1970).
[30] J. F. Fernández (private communication).
[31] F. Luis, J. Bartolomé, and J. F. Fernández, Phys. Rev. B **57**, 505 (1998); J. F. Fernández, F. Luis, and J. Bartolomé, Phys. Rev. Lett. **80**, 5659 (1998).